Structure, Chemical Bonding and ^{119}Sn Mössbauer Spectroscopy of LaRhSn and CeRhSn

Tobias Schmidt[a], Dirk Johrendt[b], C. Peter Sebastian[a], Rainer Pöttgen[a], Kazimierz Łątka[c], and Roman Kmieć[d]

[a] Institut für Anorganische und Analytische Chemie and NRW Graduate School of Chemistry, Westfälische Wilhelms-Universität Münster, Corrensstraße 30, D-48149 Münster, Germany
[b] Department Chemie und Biochemie, Ludwig-Maximilians-Universität München, Butenandtstraße 5 – 13 (Haus D), D-81377 München, Germany
[c] Marian Smoluchowski Institute of Physics, Jagiellonian University, Reymonta 4, 30-059 Kraków, Poland
[d] Henryk Niewodniczański Institute of Nuclear Physics, Polish Academy of Sciences, Radzikowskiego 152, 31-342 Kraków, Poland

Reprint requests to R. Pöttgen. E-mail: pottgen@uni-muenster.de

Z. Naturforsch. **60b,** 1036 – 1042 (2005); received August 12, 2005

The rare earth (*RE*) stannides LaRhSn and CeRhSn were prepared from the elements by arc-melting or by reactions in sealed tantalum tubes in a high-frequency furnace. The structures have been refined from X-ray single crystal diffractometer data: ZrNiAl type, $P\bar{6}2m$, $a = 748.74(5)$, $c = 422.16(3)$ pm, $wR2 = 0.0307$, 310 F^2 values for LaRhSn and $a = 745.8(1)$, $c = 408.62(9)$ pm, $wR2 = 0.0397$, 354 F^2 values for CeRhSn with 14 variables per refinement. The structures contain two crystallographically different rhodium sites which both have a tricapped trigonal prismatic coordination: [Rh1Sn$_3$*RE*$_6$] and [Rh2Sn$_6$*RE*$_3$]. Together the rhodium and tin atoms (280 – 288 pm Rh–Sn distances in LaRhSn and 277 – 285 pm in CeRhSn) build up three-dimensional [RhSn] networks in which the rare earth atoms fill distorted hexagonal channels. DFT band structure calculations reveal a large cerium $4f$ contribution at the Fermi level and a strong mixing of cerium $5d/4f$ with rhodium $4d$ orbitals. These results are in agreement with the short Ce–Rh bonds (304 and 309 pm) and also with the electronic and magnetic properties. ^{119}Sn Mössbauer spectra of LaRhSn and CeRhSn show a single tin site at isomer shifts of $\delta = 1.98(2)$ (LaRhSn) and 1.79(1) mm/s (CeRhSn) subject to quadrupole splitting of $\Delta E_Q = 0.79(4)$ (LaRhSn) and 1.12(3) mm/s (CeRhSn). The 1.8 K data show no transferred hyperfine field at the tin site for CeRhSn.

Key words: Intermetallics, Crystal Structure, Chemical Bonding, Mössbauer Spectroscopy

Introduction

The equiatomic rare earth metal (*RE*) rhodium stannides *RE*RhSn have repeatedly been investigated in the past with respect to their crystal structures and physical properties. An overview of the literature is given in [1] and [2]. Among these stannides, especially the valence fluctuating system CeRhSn [3 – 21] and antiferromagnetic YbRhSn [22 – 26] have intensively been studied.

A recent reinvestigation of the *RE*RhSn stannides with the early rare earth metals [1, 3] revealed a discrepancy for the lattice parameters. From magnetic susceptibility measurements mixed-valent behavior was evident for CeRhSn [3]. From the course of the lattice parameters given by Routsi *et al.* [3], however, no anomaly was evident for CeRhSn. Reinvestigation [1] of the lattice parameters revealed a smaller cell volume for CeRhSn as compared to PrRhSn, as expected for at least partially tetravalent cerium.

We have now investigated the structure and properties of LaRhSn and CeRhSn in more detail. Herein we report on structure refinements based on single crystal X-ray data and on a study of chemical bonding by TB-LMTO-ASA band structure calculations. Furthermore we investigated both stannides by ^{119}Sn Mössbauer spectroscopy.

Experimental Section

Synthesis

Starting materials for the preparation of LaRhSn and CeRhSn were sublimed ingots of lanthanum and cerium (Johnson Matthey), rhodium powder (Degussa-Hüls, 200 mesh), and tin granules (Merck), all with stated purities better than 99.9%. LaRhSn and CeRhSn can be prepared *via*

0932–0776 / 05 / 1000–1036 $ 06.00

arc-melting [27] or high-frequency melting [28] of the elements. For both syntheses, the rare earth pieces were first arc-melted to small buttons of about 500 mg. The argon was purified over titanium sponge (900 K), silica gel, and molecular sieves. The pre-melting procedure strongly reduces shattering during the subsequent reactions with rhodium and tin.

For the arc-melting synthesis the rare earth buttons were mixed with the rhodium powder (pressed to a pellet of 6 mm diameter) and pieces of the tin granules. The three elements were then reacted and remelted three times to ensure homogeneity. Alternatively we prepared both stannides in sealed tantalum tubes. The elements were mixed in the ideal atomic ratios, sealed in small tantalum tubes (about 1 cm^3) under an argon pressure of 600 mbar and subsequently annealed in a water-cooled sample chamber of a high-frequency furnace (Hüttinger, TIG 1.5/300) [28] under flowing argon. The tube was first heated for one minute with the maximum power output (about 1500 K), cooled to about 1100 K and annealed at about 900 K for another two hours. After the annealing procedures the samples could easily be separated from the tantalum tubes. No reactions of the samples with the tubes could be detected. Compact pieces are light gray with metallic luster. LaRhSn and CeRhSn are stable in moist air.

X-ray investigations

Both *RE*RhSn samples were characterized through powder diffractograms (Stoe StadiP) using Cu-$K_{\alpha 1}$ radiation and silicon ($a = 543.07$ pm) as an external standard. The lattice parameters were obtained from least-squares fits of the powder data and the correct indexing of the patterns was facilitated by intensity calculations [29] taking the atomic positions from the structure refinements. The parameters determined for the powdered samples and those from the single crystals agreed well.

Silvery, irregularly shaped single crystals of LaRhSn and CeRhSn were isolated from the annealed samples by mechanical fragmentation. They were examined on a Buerger precession camera in order to establish suitability for intensity data collection. Single crystal intensity data were collected at room temperature by use of a four-circle diffractometer (CAD4) with graphite monochromatized Mo-K_α radiation (71.073 pm) and a scintillation counter with pulse height discrimination. The scans were performed in the $\omega/2\theta$ mode. Empirical absorption corrections were applied on the basis of Ψ-scan data followed by spherical absorption corrections. All relevant crystallographic data and experimental details for both data collections are listed in Table 1.

Structure refinements

Analysis of the data sets showed no systematic extinctions in agreement with previous investigations [1]. Space group $P\bar{6}2m$ was found to be correct during the structure refinements. The atomic parameters of HoRhSn [1] were taken as starting values and the structures were refined using SHELXL-97 (full-matrix least-squares on $F_o{}^2$) [30] with anisotropic atomic displacement parameters for all atoms. As a check for the correct site assignment and possible Rh/Sn mixed occupancies, the occupancy parameters were refined in a separate series of least-squares cycles. All sites were fully occupied within two standard deviations. In the final cycles, the ideal occupancies were assumed. Refinement of the correct absolute structure was ensured through a refinement of the Flack parameter [31, 32]. Final difference Fourier synthesis revealed no significant residual peaks (see Table 1). The positional parameters and interatomic distances are listed in Tables 2 and 3. Further details on the structure refinements are available.*

Table 1. Crystal data and structure refinement for LaRhSn and CeRhSn, space group $P\bar{6}2m$ (No. 189), $Z = 3$.

Empirical formula	LaRhSn	CeRhSn
Molar mass [g/mol]	360.51	361.72
Unit cell dimensions (Powder data):		
a [pm]	748.74(5)	745.8(1)
c [pm]	422.16(3)	408.62(9)
V [nm^3]	0.2050	0.1968
Calculated density [g/cm^3]	8.76	9.16
Crystal size [μm^3]	$20 \times 20 \times 40$	$10 \times 20 \times 30$
Transm. ratio (max/min)	1.20	2.36
Absorption coefficient [mm^{-1}]	30.0	32.3
$F(000)$	456	459
θ Range [°]	3 to 35	3 to 35
Range in *hkl*	$\pm 10, \pm 10, \pm 4$	$\pm 12, \pm 12, +6$
Total no. reflections	657	1812
Independent reflections	310	354
$R_{\rm int}$	0.0285	0.0711
Reflections with $I > 2\sigma(I)$	294	313
R_σ	0.0343	0.0427
Data/parameters	310 / 14	354 / 14
Goodness-of-fit on F^2	0.991	1.084
Final R indices $[I > 2\sigma(I)]$	$R1 = 0.0198$	$R1 = 0.0237$
	$wR2 = 0.0294$	$wR2 = 0.0381$
R Indices (all data)	$R1 = 0.0239$	$R1 = 0.0317$
	$wR2 = 0.0307$	$wR2 = 0.0397$
Extinction coefficient	0.0085(4)	0.0060(3)
Flack parameter	$-0.03(5)$	$-0.03(5)$
Largest diff. peak and hole [$e/Å^3$]	1.31 and -1.18	1.58 and -1.66

Scanning electron microscopy

The single crystals investigated on the diffractometer have been analyzed by EDX measurements using a LEICA 420 I scanning electron microscope with LaB_6, CeO_2, rhodium, and tin as standards. No impurity elements were detected. Various point analyses on the crystals revealed the compositions 34 ± 2 at.-% La: 32 ± 2 at.-% Rh: 34 ± 2 at.-% Sn and

*Details may be obtained from: Fachinformationszentrum Karlsruhe, D-76344 Eggenstein-Leopoldshafen (Germany), by quoting the Registry No's. CSD–415594 (LaRhSn) and CSD–415595 (CeRhSn).

Atom	Wyckoff position	x	y	z	U_{11}	U_{22}	U_{33}	U_{12}	U_{eq}
LaRhSn									
La	3*f*	0.58377(9)	0	0	71(2)	84(3)	83(3)	42(1)	78(1)
Rh1	2*d*	1/3	2/3	1/2	95(3)	U_{11}	98(7)	47(1)	96(2)
Rh2	1*a*	0	0	0	83(4)	U_{11}	39(9)	41(2)	68(3)
Sn	3*g*	0.24490(9)	0	1/2	67(2)	70(3)	64(4)	35(2)	67(2)
CeRhSn									
Ce	3*f*	0.41444(11)	0	0	70(2)	80(3)	74(3)	40(2)	74(2)
Rh1	2*d*	1/3	2/3	1/2	85(3)	U_{11}	152(7)	43(2)	108(3)
Rh2	1*a*	0	0	0	83(4)	U_{11}	61(8)	41(2)	76(3)
Sn	3*g*	0.75012(10)	0	1/2	61(3)	68(4)	68(3)	34(2)	65(2)

Table 2. Atomic coordinates and anisotropic displacement parameters (pm^2) for LaRhSn and CeRhSn. U_{eq} is defined as one third of the trace of the orthogonalized U_{ij} tensor. $U_{13} = U_{23} = 0$.

Table 3. Interatomic distances (pm), calculated with the lattice parameters taken from X-ray powder data of LaRhSn and CeRhSn. All distances within the first coordination spheres are listed. Standard deviations are equal or less than 0.1 pm.

La:	4	Rh1	308.6	Ce:	4	Rh1	303.6
	1	Rh2	311.7		1	Rh2	309.1
	2	Sn	330.1		2	Sn	323.1
	4	Sn	343.7		4	Sn	338.2
	4	La	389.8		4	Ce	388.9
	2	La	422.2		2	Ce	408.6
Rh1:	3	Sn	288.4	Rh1:	3	Sn	284.9
	6	La	308.6		6	Ce	303.6
Rh2:	6	Sn	279.6	Rh2:	6	Sn	276.5
	3	La	311.6		3	Ce	309.1
Sn:	2	Rh2	279.6	Sn:	2	Rh2	276.5
	2	Rh1	288.4		2	Rh1	284.9
	2	Sn	317.6		2	Sn	322.8
	2	La	330.1		2	Ce	323.1
	4	La	343.7		4	Ce	338.2

32 ± 2 at.-% Ce: 33 ± 2 at.-% Rh: 35 ± 2 at.-% Sn, in good agreement with the ideal compositions and the results of the structure refinements. The standard uncertainties account for the various point analyses on the irregular faces of the crystals.

Electronic structure calculations

Self-consistent DFT band structure calculations were performed using the LMTO-method in its scalar-relativistic version (program TB-LMTO-ASA) [33]. Detailed descriptions are given elsewhere [34, 35]. Reciprocal space integrations were performed with the tetrahedron method [36] using 666 *k*-points within the irreducible wedge of the hexagonal Brillouin zone, which was divided in a $11 \times 11 \times 11$ mesh. The basis set consisted of Ce: $6s/\{6p\}/5d/4f$, Rh: $5s/5p/4d/\{4f\}$, and Sn: $5s/5p/\{5d/4f\}$. Orbitals given in parentheses were downfolded [37]. In order to achieve space filling within the atomic sphere approximation, interstitial spheres are introduced to avoid too large overlap of the atom-centered spheres. The empty spheres positions and radii were calculated automatically. We did not allow overlaps of more than 15% for any two atom centered spheres. The COHP method was used for the bond analysis [38]. COHP gives the energy contributions of all electronic states for a selected bond. The values are negative for bonding and positive for antibonding interactions. With respect to the COOP diagrams, we plot –COHP(E) to get positive values for bonding states.

^{119}*Sn Mössbauer spectroscopy*

A $Ca^{119m}SnO_3$ source was available for the ^{119}Sn Mössbauer spectroscopic investigations. The samples were placed within thin-walled PVC containers at a thickness of about 10 mg Sn/cm^2. A palladium foil of 0.05 mm thickness was used to reduce the tin K X-rays concurrently emitted by this source. The measurements were conducted in the usual transmission geometry at room temperature, 78 K, and 1.8 K. Transmission integral fits were obtained using the Levenberg-Marquard algorithm, resulting in the parameters of isomer shift, electric quadrupole splitting, and line width.

Discussion

Crystal chemistry and chemical bonding

The stannides LaRhSn and CeRhSn have been structurally characterized on the basis of single crystal X-ray diffractometer data. In parallel to our investigations [10], the CeRhSn structure was also investigated by Kim *et al.* [11] from an inversion twin and by Ślebarski *et al.* [5] by neutron powder diffraction, while so far, LaRhSn has only been characterized on the basis of X-ray powder data [39]. The single crystal and powder diffraction data from [5] and [11] are in good agreement with the data presented here. In the following discussion section we focus only on the cerium compound.

At this point we need to discuss the anisotropic displacement parameters of the *RE*RhSn stannides. For *RE* = Gd–Lu, the Rh2 atoms at the origin of the cell show significant displacements in the *c*-direction [1], *i.e.* the U_{33} value is up to six times larger than the U_{11} value. The structures with the larger rare earth elements, *i.e.* LaRhSn (Table 2), PrRhSn [40], and

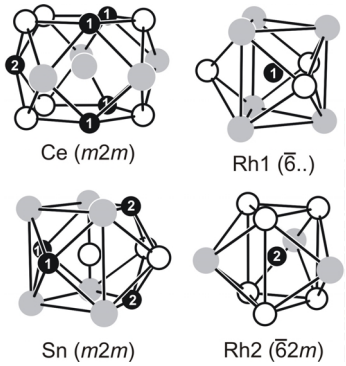

Fig. 1. Coordination polyhedra in the CeRhSn structure. The site symmetries are indicated.

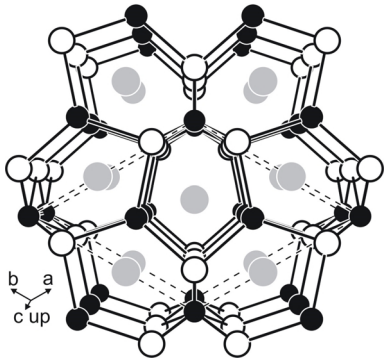

Fig. 2. View of the CeRhSn structure along the *c* axis. Cerium, rhodium, and tin atoms are drawn as gray, filled, and open circles, respectively. The three-dimensional [RhSn] network is emphasized.

NdRhSn [41], however, do no show these anomalies. The situation is even more different for CeRhSn. Due to the intermediate valence, the *c* parameter shows a significant anomaly (smaller than that of NdRhSn) in the plot of the cell volumes of the *RE*RhSn series [1]. Consequently, the trigonal prisms around the rhodium atoms are compressed. Here, the U_{33} parameter of Rh1 is about two-times larger. If such displacements are very large, a superstructure can form upon doubling of the *c* axis, similar to HfRhSn [42]. For CeRhSn, however, neither superstructure reflections nor diffuse scattering have been observed.

CeRhSn adopts the well known ZrNiAl type [43–45] structure. Since the crystal chemistry of this structure type has intensively been discussed in previous papers [1, 42, and ref. therein], we give only a brief description here. In Figures 1 and 2 we present the coordination polyhedra and a perspective view of the CeRhSn structure. The cerium atoms have coordination number 15 (pentacapped pentagonal prism) with 4 Ce, 5 Rh, and 6 Sn atoms in their coordination shell. Two further cerium atoms are capping the pentagonal faces at a Ce–Ce distance of 409 pm which corresponds to the *c* translation period. The shortest Ce–Ce distance in CeRhSn is 389 pm, significantly longer than the Hill limit [46] of about 340 pm for *f* electron localization, however, no magnetic ordering is observed for this stannide. In the isotypic magnesium compounds Ce*T*Mg (T = Pd, Pt, Au), the Ce–Ce distances are 399, 394, and 404 pm, respectively. For these intermetallics long-range magnetic ordering has been observed [47]. In this context it is interesting to note that CeRhMg [48] (Ce–Ce 392 pm) also crystallizes with the ZrNiAl type structure. In contrast to CeRhSn, a homogeneity range $CeRh_{1+x}Mg_{1-x}$ has been observed. The magnetic properties of CeRhMg, however, have not yet been investigated.

The shortest interatomic distances in CeRhSn occur for the Rh–Sn contacts, 277 – 285 pm, slightly longer than the sum of the covalent radii of 265 pm [49]. Also the Sn–Sn distances (323 pm) within the triangular faces of the trigonal prisms around the Rh2 atoms are short. They compare well with the Sn–Sn distances in β-tin (four neighbors at 302 pm and two further neighbors at 318 pm) [50]. Based on a comparison of these interatomic distances, we can describe the CeRhSn structure with a three-dimensional [RhSn] network in which the cerium atoms fill distorted hexagonal channels as outlined in Fig. 2.

Striking features are certainly the relatively short Ce–Rh distances of 304 and 309 pm. These are between the sums of the covalent and metallic [49] radii of 290 and 317 pm, respectively. Similar short Ce–Rh distances were recently also observed in $Ce_2Rh_{1.86}Cd$ (284 – 300 pm) [51]. We can thus assume significant Ce–Rh bonding in both compounds.

For a more detailed view of chemical bonding in CeRhSn we performed electronic structure calculations with the TB-LMTO-ASA technique. The total electronic density-of-states (DOS) is depicted in Fig. 3a together with the partial DOS of cerium, rhodium and tin, respectively. Spin polarized calculations converged back to a nonmagnetic ground state, in agreement with the intermediate-valent character observed from the magnetic data [3, 5, 10]. According to the metallic property of CeRhSn, no gap is discernible at the Fermi level (E_F). The DOS value at E_F is 2.16 states/eV·formula, which is about 20% larger

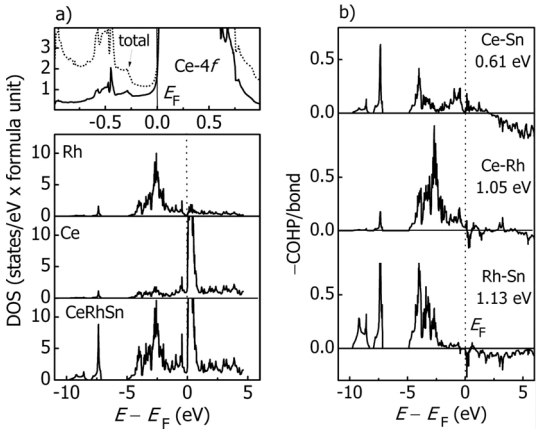

Fig. 3. a) Total and partial density-of-states (DOS) of CeRhSn. The uppermost diagram shows details of the DOS in the vicinity of the Fermi level. b) Crystal Orbital Hamilton Populations (COHP) of selected bonds in CeRhSn. Each diagram represents the weighted average over bonds of the same kind. The mean ICOHP bonding energy is given in eV/bond.

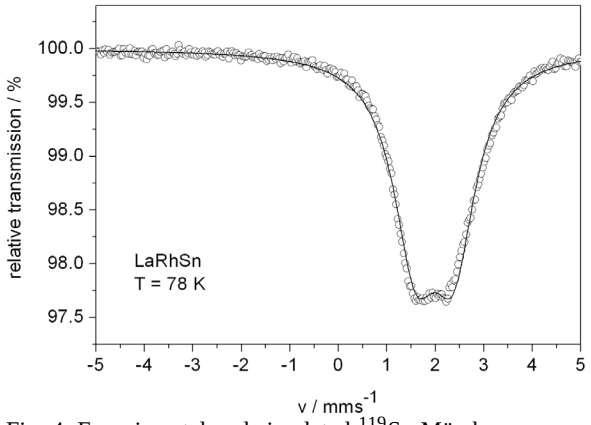

Fig. 4. Experimental and simulated ^{119}Sn Mössbauer spectrum of LaRhSn at 78 K.

than the value reported in ref. [7]. Apart from this relatively small difference, the DOS agrees almost exactly with that from previous calculations [7, 9, 20]. A closer inspection (see the uppermost diagram of Fig. 3a) reveals that the DOS at E_F is mainly determined by the cerium $5d/4f$ levels, which contribute about 88%, whereas rhodium and tin supply only 9% and 3%, respectively. Furthermore, the DOS increases drastically at E_F, which lies narrowly at the bottom of the $4f$ peak. However, this explains the different DOS values, because it is difficult to calculate an accurate value for the DOS at E_F where the slope is so large. On the other side, this result indicates, that the remarkable physical properties regarding transport and magnetism are clearly connected with a significant degree of hybridization of the $4f$ states with the conduction electrons. To analyze the chemical bonding, we present the COHP diagrams of the Ce–Sn, Ce–Rh and Rh–Sn bonds in Fig. 3b. The Ce–Rh and Rh–Sn bonding states are completely occupied and these bonds are by far the strongest. It is remarkable that the Ce–Rh covalent ICOHP bonding energy is almost as large as that of Rh–Sn and differs by only 7.5%. This is in good agreement with the relatively short Ce–Rh distances and indicates again a strong mixing of the cerium $5d/4f$ with the rhodium 4*d* orbitals. The COHP of the Ce–Rh bonds in CeRhSn differs considerably from the Ce–Pt bonds in isostructural HP-CePtSn [52], even though the resulting ICOHP bonding energy is similar. The platinum 5*d* orbitals are lower in energy and – owing to the nearly d^{10} configuration – much more spatially contracted than the rhodium 4*d*. Thus, one can expect that the mixing of the transition metal *d*-block with the cerium $4f$ is much more distinct in CeRhSn than in HP-CePtSn. This explains the strong Ce–Rh bonds and may also be an important precondition for the remarkable physical properties of CeRhSn from a chemical point of view.

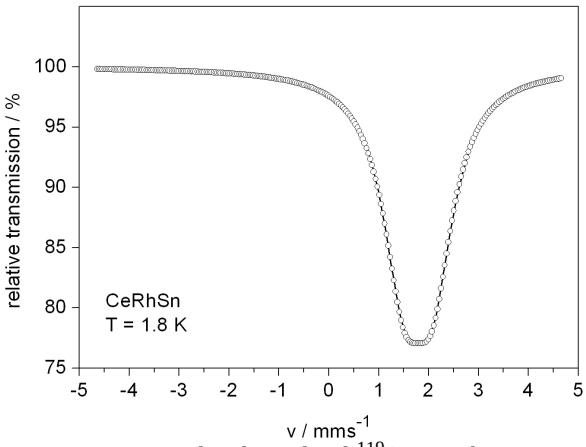

Fig. 5. Experimental and simulated ^{119}Sn Mössbauer spectrum of CeRhSn at 1.8 K.

^{119}*Sn Mössbauer spectroscopy*

Figures 4 and 5 show the ^{119}Sn Mössbauer spectra of LaRhSn and CeRhSn. In agreement with the structure refinements, both spectra show only one tin signal at isomer shifts of $\delta = 1.98(2)$ (LaRhSn) and 1.81(1) mm/s (CeRhSn) subject to quadrupole splitting of $\Delta E_Q = 0.79(4)$ (LaRhSn) and

1.12(3) mm/s (CeRhSn). The experimentally determined line widths are $W = \Gamma_s + \Gamma_a = 1.11(7)$ (LaRhSn) and 0.94(1) (mm/s (CeRhSn). These values are close to the recently reported Mössbauer data for PrRhSn [40] and NdRhSn [41], and for the *RE*RhSn stannides with the heavier rare earth elements [1, 2]. The 1.8 K data show no transferred hyperfine field for CeRhSn, in agreement with the non-magnetic ground state observed from the susceptibility measurements [10] and the electronic structure calculations.

Acknowledgements

We thank Dipl.-Ing. U. Ch. Rodewald for the intensity data collection and the Degussa-Hüls AG for a generous gift of rhodium powder. This work was supported by the Deutsche Forschungsgemeinschaft and by Poland's Committee for Scientific Research grant under contract No: 1 P03B 084 28. C.P.S. is indebted to the NRW Graduate School of Chemistry for a PhD stipend.

[1] R. Mishra, R. Pöttgen, R.-D. Hoffmann, H. Trill, B. D. Mosel, H. Piotrowski, M. F. Zumdick, Z. Naturforsch. **56b**, 589 (2001).
[2] K. Łątka, R. Kmieć, R. Kruk, A. W. Pacyna, Th. Fickenscher, R.-D. Hoffmann, R. Pöttgen, J. Solid State Chem. **178**, 2077 (2005).
[3] Ch. D. Routsi, J. K. Yakinthos, H. Gamari-Seale, J. Magn. Magn. Mater. **117**, 79 (1992).
[4] Y. Bando, T. Suemitsu, K. Takagi, H. Tokushima, Y. Echizen, K. Katoh, K. Uemo, Y. Maeda, T. Takabatake, J. Alloys Compd. **313**, 1 (2000).
[5] A. Ślebarski, M. B. Maple, E. J. Freeman, C. Sirvent, M. Radłowska, A. Jezierski, E. Granado, Q. Huang, J. W. Lynn, Philos. Mag. B **82**, 943 (2002).
[6] A. Ślebarski, N. A. Frederick, M. B. Maple, Philos. Mag. B **82**, 1275 (2002).
[7] A. Ślebarski, M. Radłowska, T. Zawada, M. B. Maple, A. Jezierski, A. Zygmunt, Phys. Rev. B **66**, 104434 (2002).
[8] Y. Echizen, K. Yamane, T. Takabatake, Physica B **329–333**, 522 (2003).
[9] A. Ślebarski, A. Jezierski, Phys. Stat. Sol. B **236**, 340 (2003).
[10] K. Łątka, M. Rams, R. Kmieć, R. Kruk, A. W. Pacyna, T. Schmidt, G. Kotzyba, R. Pöttgen, D. Johrendt, Acta Phys. Pol. **34**, 1225 (2003).
[11] M. S. Kim, Y. Echizen, K. Umeo, S. Kobayashi, M. Sera, P. S. Salamakha, O. L. Sologub, T. Takabatake, X. Chen, T. Tayama, T. Sakakibara, M. H. Jung, M. B. Maple, Phys. Rev. B **68**, 054416 (2003).
[12] K. Łątka, R. Kmieć, R. Kruk, A. W. Pacyna, M. Rams, T. Schmidt, R. Pöttgen, Nukleonika **48(Suppl.)**, S35 (2003).
[13] M. S. Kim, Y. Echizen, K. Umeo, T. Tayama, T. Sakakibara, T. Takabatake, Physica B **329 – 333**, 524 (2003).
[14] M. S. Kim, T. Sasakawa, Y. Echizen, T. Takabatake, Jpn. J. Appl. Phys. **42**, 6512 (2003).
[15] A. Schenck, F. N. Gygax, M. S. Kim, T. Takabatake, J. Phys. Soc. Jpn. **73**, 3099 (2004).
[16] A. Ślebarski, K. Grube, R. Lortz, C. Meingast, H. v. Löhneysen, J. Magn. Magn. Mater. **272–276**, 234 (2004).
[17] T. Suzuki, H. Higaki, I. Ishii, M. S. Kim, T. Takabatake, J. Magn. Magn. Mater. **272 – 276**, e35 (2004).
[18] P.-C. Ho, V. S. Zapf, A. Ślebarski, M. B. Maple, Phil. Mag. **84**, 2119 (2004).
[19] H. Tou, M. S. Kim, T. Takabatake, M. Sera, Phys. Rev. B **70**, 100407 (2004).
[20] A. Ślebarski, T. Zawada, J. Spałek, A. Jezierski, Phys. Rev. B **70**, 235112 (2004).
[21] A. Ślebarski, T. Zawada, J. Spałek, Physica B **359 – 361**, 118 (2005).
[22] D. Kaczorowski, A. Leithe-Jasper, P. Rogl, H. Flandorfer, T. Cichorek, R. Pietri, B. Andraka, Phys. Rev. B **60**, 422 (1999).
[23] K. Katoh, G. Terui, Y. Niide, H. Aoki, A. Ochiai, Physica B **259-261**, 161 (1999).
[24] O. Trovarelli, C. Geibel, R. Cardoso, S. Mederle, R. Borth, B. Buschinger, F. M. Grosche, Y. Grin, G. Sparn, F. Steglich, Phys. Rev. B **61**, 9467 (2000).
[25] R. Pietri, B. Andraka, D. Kaczorowski, A. Leithe-Jasper, P. Rogl, Phys. Rev. B **61**, 12169 (2000).
[26] B. Andraka, R. Pietri, D. Kaczorowski, A. Leithe-Jasper, P. Rogl, J. Appl. Phys. **87**, 5149 (2000).
[27] R. Pöttgen, Th. Gulden, A. Simon, GIT-Laborfachzeitschrift **43**, 133 (1999).
[28] D. Kußmann, R.-D. Hoffmann, R. Pöttgen, Z. Anorg. Allg. Chem. **624**, 1727 (1998).
[29] K. Yvon, W. Jeitschko, E. Parthé, J. Appl. Crystallogr. **10**, 73 (1977).
[30] G. M. Sheldrick, SHELXL-97, Program for Crystal Structure Refinement, University of Göttingen, Germany (1997).
[31] H. D. Flack, G. Bernadinelli, Acta Crystallogr. **55A**, 908 (1999).
[32] H. D. Flack, G. Bernadinelli, J. Appl. Crystallogr. **33**, 1143 (2000).
[33] O. K. Andersen, O. Jepsen, Tight-Binding LMTO Vers. 4.7, Max-Planck-Institut für Festkörperforschung, Stuttgart (1994).
[34] O. Jepsen, M. Snob, O. K. Andersen, Linearized Band Structure Methods and its Applications, Springer Lecture Notes, Springer-Verlag, Berlin (1987).

[35] H. L. Skriver, The LMTO Method, Springer-Verlag, Berlin (1984).
[36] O. K. Andersen, O. Jepsen, Solid State Commun. **9**, 1763 (1971).
[37] W. R. L. Lambrecht, O. K. Andersen, Phys. Rev. B **34**, 2439 (1986).
[38] R. Dronskowski, P. Blöchl, J. Phys. Chem. **97**, 8617 (1993).
[39] F. Canepa, S. Cirafici, J. Alloys Compd. **232**, 71 (1996).
[40] K. Łątka, R. Kmieć, R. Kruk, A. W. Pacyna, T. Schmidt, R. Pöttgen, J. Solid State Chem. **178**, 3101 (2005).
[41] K. Łątka, R. Kmieć, J. Gurgul, A. W. Pacyna, M. Rams, T. Schmidt, R. Pöttgen, J. Magn. Magn. Mater., in press.
[42] M. F. Zumdick, R. Pöttgen, Z. Kristallogr. **214**, 90 (1999).
[43] P. I. Krypyakevich, V. Ya. Markiv, E. V. Melnyk, Dopov. Akad. Nauk. Ukr. RSR, Ser. A 750 (1967).
[44] A. E. Dwight, M. H. Mueller, R. A. Conner (Jr.), J. W. Downey, H. Knott, Trans. Met. Soc. AIME **242**, 2075 (1968).
[45] M. F. Zumdick, R.-D. Hoffmann, R. Pöttgen, Z. Naturforsch. **54b**, 45 (1999).
[46] H. H. Hill, in W. N. Mines (ed.): Plutonium and Other Actinides, Nuclear Materials Series, Vol. 17, p. 2, AIME, New York (1970).
[47] B. J. Gibson, A. Das, R. K. Kremer, R.-D. Hoffmann, R. Pöttgen, J. Phys. Condens. Matter. **14**, 5173 (2002).
[48] Th. Fickenscher, R.-D. Hoffmann, R. Kraft, R. Pöttgen, Z. Anorg. Allg. Chem. **628**, 667 (2002).
[49] J. Emsley, The Elements, 3rd edn, Oxford University Press, Oxford (1999).
[50] J. Donohue, The Structures of the Elements, Wiley, New York (1974).
[51] F. Stadler, Th. Fickenscher, R. Pöttgen, Z. Naturforsch. **56b**, 1241 (2001).
[52] J. F. Riecken, G. Heymann, Th. Soltner, R.-D. Hoffmann, H. Huppertz, D. Johrendt, R. Pöttgen, Z. Naturforsch. **60b**, 821 (2005).